





# A Computational Approach for Contactless Muscle Force and Strain Estimations in Distributed Actuation Biohybrid Mesh Constructs

Saul Schaffer<sup>(✉)</sup> , Janice Seungyeon Lee, Lameck Beni,  
and Victoria A. Webster-Wood 

Carnegie Mellon University, 5000 Forbes Ave, Pittsburgh, PA 15213, USA  
[biorobot@cmu.edu](mailto:biorobot@cmu.edu), [vwebster@andrew.cmu.edu](mailto:vwebster@andrew.cmu.edu)  
<http://engineering.cmu.edu/borg>

**Abstract.** Biological muscle tissue can adapt to mechanical stimuli such as strain and become stronger. While this property has been explored for single, independent muscle actuators, it is still not well understood for more complex, distributed actuation architectures, which are needed for more complex biohybrid robotic systems. This study presents a computational approach for contactless methods to estimate individual muscle actuator strains and individual muscle forces on a distributed-actuator biohybrid mesh substrate. The methods presented in this work estimate the strain each muscle experiences as the substrate is stretched by creating a finite element model of our distributed muscle actuator biohybrid mesh, taking  $79.8 \pm 51.9$  s to compute. Additionally, two contactless methods for muscle force estimation based on patterned substrate deformation are presented and compared: 1) Response Surface optimization, and 2) Direct Optimization. Both force estimation methods extract distributed muscle forces based on global substrate deformations. The Response Surface optimization resulted in a prediction error of  $321 \pm 219 \mu\text{m}$  with a runtime after model creation of  $26 \pm 1.3$  s. The Direct Optimization method resulted in a prediction error of  $0 \mu\text{m}$  but took a long, highly-variable runtime of  $663.4 \pm 918.5$  s. Directions for further improvement are discussed. Towards experimental validation of the outlined computational tools, a biaxial stretcher was constructed, and the ability to command desired displacements with the apparatus was characterized. The biaxial stretching platform achieved an average precision error of  $3.10 \pm 5.92\%$  and  $5.34 \pm 2.38\%$  for the x- and y-bars, respectively. Our methods aim to fill a critical gap in the design and analysis capabilities available to biohybrid robotics researchers. These preliminary estimation methods indicate the feasibility of our contactless muscle strain and muscle force estimation paradigm, which will be used to inform future *in vitro* experiments.

**Keywords:** Biohybrid · Distributed actuation · Mesh · Biohybrid muscle training · Computational tool

# 1 Introduction

Soft robots with bioinspired distributed actuation schemes show great promise for tasks that require navigating tight spaces. Using their high number of degrees of freedom, systems like the MIT Meshworm [25] and the CWRU Meshworm [6, 13] are able to contort their structures to squeeze through otherwise inaccessible spaces, with promising use cases in pipe inspection [10] as well as search and rescue and medicine. However, robots built with traditional materials are limited in how far they can be scaled down, as there is a lack of soft microactuators available to drive sufficiently small, soft systems [23, 30].

Fortunately, biological muscle actuators are able to operate at significantly smaller scales than those achievable with current synthetic actuators [23]. Additionally, muscle actuators can endow robotic systems with desirable capabilities such as high compliance [16, 30], self-healing [21], and biocompatibility [23, 30]. Using muscle tissue as an actuator, researchers have demonstrated inchworm locomotion [7, 28], jellyfish [19], ray-like [17], and fish swimming [14], as well as rudimentary manipulation [16]. Using a biohybrid paradigm, researchers could develop trainable, behaviorally flexible, biocompatible systems that could adapt to dynamic environments beyond the lab. Long-term applications of such systems include medical applications, such as robotic stents (Fig. 1d–e) that are able to travel inside a patient’s blood vessels with earthworm-inspired peristaltic locomotion and deploy themselves at the site of arterial blockages.

While impressive, the capabilities of biohybrid robots—those that leverage both living and synthetic materials—remain much less sophisticated than traditional robots. One reason for this is that muscle actuators adapt to their environment, which means they will change their properties during use. Such adaptation makes the modeling and design of complex biohybrid systems quite challenging [23, 30]. One such example of adaptation is seen when muscle actuators experience tensile strain either through activation or external stretching. Under such loading, muscles become stronger, producing more force [8, 11, 15, 18, 20, 22, 26]. While this property of muscle is well known, this relationship between the strain the muscle experiences and the resulting increase in force they are able to produce in distributed multi-actuator systems is not well understood and has led to the state-of-the-art in biohybrid robotics being low degree-of-freedom, lab-chained devices [16, 23, 30]. However, just as in synthetic robots, distributed actuation in biohybrid robots has great promise for future applications.

Mesh-based biohybrid architectures (Fig. 1a–c) can serve as a platform to study muscle adaptability in distributed actuation biohybrid systems, an important step in the development of more functional, complex biohybrid systems. However, the strains muscle actuators would experience in a distributed architecture, like the mesh substrate illustrated in Fig. 1, are challenging to measure directly, as are the forces the muscle actuators produce. These challenges arise from the fragility of the muscle actuators, their low force output, and their adaptation to the mechanical stimulus present in the muscle’s environment [23].

To study the effects of exercise in biohybrid distributed actuation architectures, there is a need to know the strains individual muscles experience on a

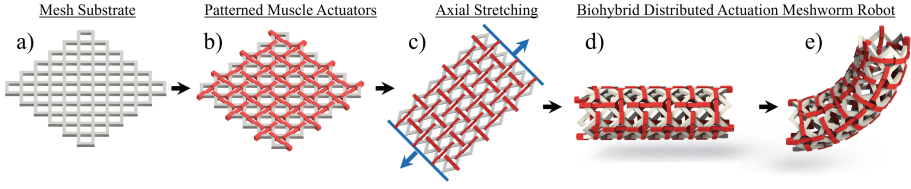


**Fig. 1.** Concept of distributed actuation biohybrid meshworm. **a)** Mesh substrate. **b)** Muscles patterned on the substrate, forming a 2D biohybrid distributed actuation construct. **c)** Biohybrid construct subjected to strain exercise training. **d)** 2D construct is wrapped into biohybrid meshworm robot. **e)** Biohybrid meshworm robot bending through selective activation of the muscle actuators patterned on the substrate.

stretched mesh (Fig. 1c). Due to the mesh’s anisotropic deformation and loading conditions, individual muscles on the same mesh will experience different amounts of strain depending on where they are located. Previous studies have shown muscle maturation is sensitive to this strain, with muscles that experience more strain becoming stronger as a result [20]. Therefore, understanding the experienced strain of each muscle on the mesh substrate is critical for elucidating the effects of strain loading on muscle force development.

A second critical factor for studying the effects of exercise on a biohybrid distributed actuation system is the output force of individual muscles. The computational estimation methods presented here are designed to enable future *in vitro* experiments investigating the relationship between muscle strain and muscle force. As such, the material models, geometries, and boundary conditions are all reflections of what will be embodied in those experiments. It is also important that these computational tools be efficient and accurate so that they can be used to aid future researchers in designing more complex biohybrid systems.

This work presents a set of computational tools for estimating strains experienced and forces produced by distributed muscle actuators patterned on a biohybrid mesh substrate. The first section details a contactless method for estimating muscle strain on a stretched mesh. The second section details and compares two approaches to contactless force estimation, which will equip future *in vitro* experiments with the ability to characterize the relationship between experienced muscle strain during maturation and increased mature muscle force production. Lastly, we showcase preliminary work towards physical experiments validating our computational tools in the form of characterizing a biaxial stretcher.

## 2 Methods

To address the need for contactless strain and force estimation for distributed actuator biohybrid mesh-based systems (Fig. 2a), a suite of computational methods were developed. These methods were created to supplement future *in vitro* experiments by quantifying the relationship between muscle strain and muscle force on a distributed actuation system using optimization tools in ANSYS

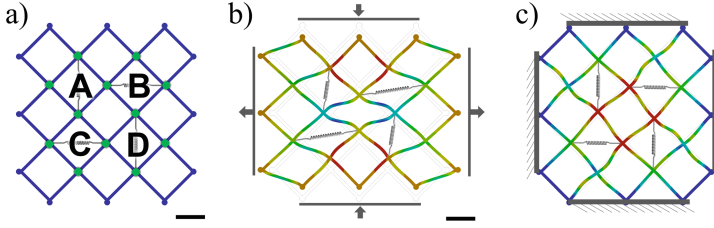


**Fig. 2.** **a)** Mesh substrate (*blue*) with patterned muscle actuators A-D (*grey springs*) connecting adjacent nodes (*green dots*) of the mesh. **b)** Loading conditions for mesh substrate when stretched, implemented in strain estimation method. Mesh deforms from external stretching loads. **c)** Loading conditions for force estimation methods. Mesh construct deforms under action of the muscles contracting, mesh is fixed on all sides. All mesh deformations are to scale, and all scale bars are 5 mm. (Color figure online)

Workbench 2021 R2 (Canonsburg, PA, USA). For this preliminary study, the mesh substrate is assigned an elastic modulus of 250 kPa and a Poisson's ratio of 0.499, as an idealized linear elastic model of collagen, a common structural biomaterial [12] used in biohybrid robotics [29]. Furthermore, a mesh convergence study was conducted, resulting in the selection of an element size of 400  $\mu\text{m}$  (13,441 elements). Subsequently, the finite element mesh was automatically generated in ANSYS using Program Controlled element order and triangular surface mesher. Simulations were performed with Large Deflections enabled and Solver Type set to "Direct".

## 2.1 Contactless Estimation of Distributed Muscle Strain

To understand the effect of muscle strain on muscle force, it is critical to quantify the strain experienced by muscles as the substrate on which they are patterned is stretched (Fig. 2b). The stretch loading conditions of the construct were determined by the capabilities of a modified open-source biaxial stretcher [26]. We hypothesized that the strain experienced by the muscles is not a constant scalar multiple of the stretch imposed on the mesh. Instead, we posit that the strains experienced by the patterned muscles depend not only on the stretch imposed on the mesh but also on the muscle alignment to the stretch orientation, as well as the distance the muscles are placed from the center of the mesh. To test this hypothesis, a finite element model that tracks the relative displacement between mesh nodes (Fig. 2a) corresponding to muscle attachment points was developed. As the construct was subjected to a prescribed external displacement load (Fig. 2b), the muscles stretched and shrank depending on their location and orientation on the substrate. The strain estimations for each potential muscle actuator was implemented by estimating the strain of negligibly soft springs ( $k_{spring} < 10^{-14} \mu\text{N/mm}$ ) attached between these nodes. As the nodes moved relative to each other, these virtual strain gauges enabled tracking of the strain a muscle actuator would have experienced if patterned between those nodes.

## 2.2 Contactless Estimation of Distributed Muscle Force

Equipped with a tool to determine the strain individual muscles experience on a stretched mesh construct, a method for estimating the forces those muscles produce is needed to ascertain the relationship between muscle strain loading during maturation and muscle force. Potential force estimation tools need to meet two key criteria to be useful for this endeavor. First, the method should estimate the force generated by distributed muscle actuators *in vitro* without physically contacting the muscles. This is because removing the muscles from the environment in which they are grown to measure their force has the chance to damage the muscle and/or change how the muscle might have performed if left *in situ*. Furthermore, any additional mechanical contact with the mesh during culture may alter the loading condition experienced by the muscles. Secondly, a useful force estimation method needs to allow for multiple muscle forces to be estimated simultaneously, especially when these muscles are mechanically coupled, as in a distributed actuation mesh (Fig. 1a–c). One such approach to estimating muscle forces that satisfies these criteria is to have the substrate on which the muscles are patterned act as a force gauge. By optically quantifying the deformation of the substrate under the action of the muscles patterned on it, we hypothesize that we can estimate the forces those patterned muscles are producing. Presented here are two computational methods based on this approach, namely Response Surface Optimization and Direct Optimization. All the mesh deformations described here were generated from a finite element model of the system with assumed muscle forces. However, in an experimental setup, mesh deformation estimations would be found by taking optical images of the biohybrid construct and using digital image correlation methods [27] to estimate the mesh deformation under the action of the muscles. The possible muscle forces used for each actuator was 0–8,000  $\mu\text{N}$ , which is within the range of actuator forces expected from the literature from a muscle of 0.4 mm thick and 5 mm wide [7, 9, 18, 21, 24]. As the goal of these estimation methods is to become fast and accurate tools for distributed actuation biohybrid robot design and analysis, computational runtime was recorded for all methods, both in method setup or training and method implementation.

**Response Surface Optimization Force Estimation.** The first method tested for estimating muscle forces from mesh deformation was centered around creating a continuous response surface mapping from patterned muscle forces to mesh deformation (Fig. 3). Once the response surface was established, a multi-objective optimization problem was set up that searches on the response surface for a muscle force set that produces a mesh deformation closest to a specific input mesh deformation. With this approach, mesh deformations were input to the Response Surface optimization method, which would output its optimal estimation for the corresponding muscle forces. The response surface was trained with 200 sets of input muscle forces for muscles A–D (Fig. 2a) and generated using the Genetic Aggregation algorithm available in the ANSYS DesignXplorer suite [2]. In brief, Genetic Aggregation uses a genetic algorithm to configure, generate, evaluate, and evolve populations of response surfaces, drawing from the

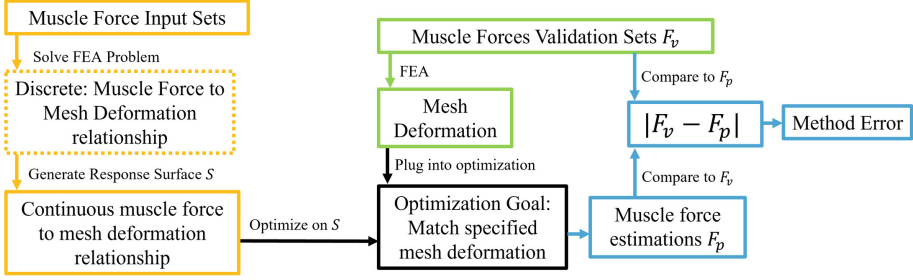


**Fig. 3.** Flow diagrams for Response Surface Optimization method: Generate response surface (yellow), search (black) for optimal muscle forceS given a deformation (green). (Color figure online)

set of response surface types available in ANSYS (e.g. Full 2nd-Order Polynomials, Non-Parametric Regression, and Kriging). The fitness of a given response surface was determined in part by the fidelity of the response surface to data it is representing. Genetic Aggregation was selected as it is more reliable than the other response surface generation algorithms, while taking more time [5]. Once the response surface was generated, the Multi-Objective Genetic Algorithm (MOGA) was selected as the goal-driven optimization method to find muscle force estimation sets. This method generates populations of muscle force sets and evaluates their outputs on the response surface with a fitness function [3], iteratively improving the muscle force set estimations by subsequently generating evolved populations through cross-over and mutation of the fittest estimations [4]. MOGA converged when the mean and standard deviation of the output parameters of successive populations were within 2%.

**Direct Optimization Force Estimation.** An alternate approach to the Response Surface method is to perform Direct Optimization (Fig. 4). Rather than generating a response surface, Direct Optimization directly implements MOGA, solving the finite element problem for guesses of muscle force sets that iteratively reducing the error between the input mesh deformation and the finite element solution mesh deformation. MOGA for Direct Optimization also converged when the mean and standard deviation of the output parameters of successive populations were within 2%.

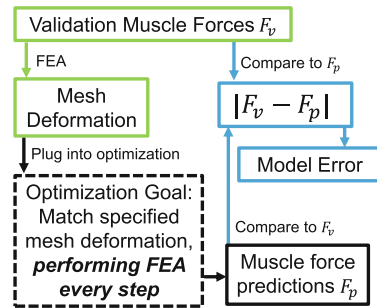


**Fig. 4.** Direct optimization method: search (black) for muscle force values given a deformation (green). Method error is quantified (blue). The dashed block is the most computationally expensive. (Color figure online)

### 2.3 Characterization of a Biaxial Stretching Platform Towards *In Vitro* Validation

Experimental validation of the outlined computational tools requires a physical apparatus to impose known strains on a mesh construct. Towards future experimental validation, a biaxial stretcher [26] was constructed, and the ability to command desired displacements with the apparatus was characterized. This characterization was conducted by analyzing the actual displacement of each attachment bar of the biaxial stretcher given a desired displacement. The biaxial stretcher is attached to a metal frame with a camera mounted directly above the stretcher (Fig. 7a). This biaxial stretcher has four attachment bars, two that move in the x-axis and two in the y-axis (Fig. 7b). These bars move an equal distance away or towards each other, creating a stretching or contracting motion. The stretcher is controlled by gcode on a Duet WiFi board (Duet3D). During operation, the camera records 15 s of the bar oscillations for a given displacement. Five commanded displacement were tested: 5, 10, 15, and 20 mm. To facilitate motion tracking, labeled dots were mounted on each attachment bar. The actual displacements of each bar were then determined using the “Tracker” software [1]. It was noted that the displacements commanded in gcode differed from the displacements achieved by the bars of the apparatus. Thus, we developed a method of generating adjustment ratios to achieve the desired displacements. Two adjustment ratios approaches were tested, uniform and displacement-specific ratio values. The uniform ratio was found using the `polyfit()` function from MATLAB (MathWorks, Natick, MA, USA) with  $n = 1$  for each of the four attachment bars and averaging for x- and y-axis independently. The displacement-specific ratio was found by averaging the value from each of the two bars in the x- and y-axis, respectively. We adjusted the input displacement values by dividing the identified ratio value when writing the gcode that commands the biaxial stretcher. The difference in the actual displacement and desired displacement was then used to adjust the gcode to match the input displacement and the actual displacement. The remaining deviation at each displacement was measured experimentally using both adjustment ratios, and the ratio with lower error for each displacement was determined for further use.

### 2.4 Statistical Analysis of Contactless Force and Strain Estimation Methods

For each muscle force estimation method, performance was calculated for 10 sets of computationally generated validation muscle force sets, where each set considered muscles A–D independently (Fig. 2a). A one-way ANOVA was conducted to determine if there was a difference in force estimation error between individual muscles (A, B, C, D) for the Response Surface method. Additionally, a one-way ANOVA was conducted to compare the force estimation error between the Response Surface and Direct Optimization methods, aggregating muscle force estimation errors across muscles. Statistical significance was determined by  $p < 0.001$ . All analysis was performed in MATLAB.



### 3 Results and Discussion

#### 3.1 Muscle Strain Estimation

As hypothesized, the muscle strain estimation method showed a relationship between *i)* the muscle orientation relative to stretch direction and *ii)* muscle placement on the muscle strain. For each muscle, maximum strain was achieved when maximum positive stretch was applied in the direction of the muscle's orientation and maximum compressive displacement – 'negative stretch' – was applied perpendicular to that orientation (Fig. 5). In future *in vitro* experiments, this negative stretch would result in the unloading of those muscles. Additionally, we found that muscles placed in the center of the mesh would experience more strain than elsewhere. Each muscle strain estimation took  $79.8 \pm 51.9$  s to simulate a set of four muscles, with  $n = 10$ .

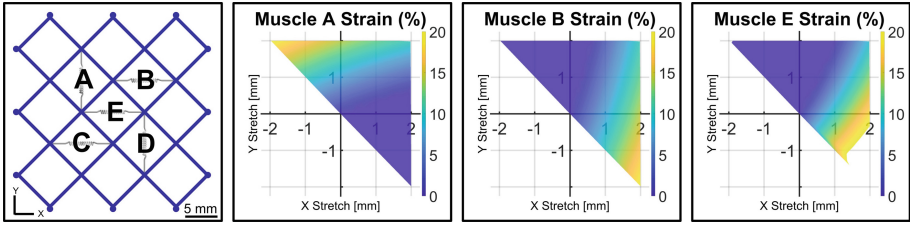


**Fig. 5.** Strain experienced by individual muscle actuators subjected to biaxial stretching, where positive stretch indicates tension. Plots for Muscles A and B (shown) are the same as Muscles D and C (not shown), respectively. Maximum strain values for Muscles A, B, C, D and E are 19.48%, 19.47%, 19.60%, 19.52%, and 28.13%, respectively. Color bar unit is percent strain.

#### 3.2 Muscle Force Estimation

To evaluate the performance of the muscle force estimation methods, we generated mesh deformations from validation muscle force sets that were not used in Response Surface generation. The force estimation methods were used to estimate what forces were required to generate those deformations. Force estimation method error was calculated for 10 sets of muscle forces by taking the magnitude of the difference between the force estimations and the forces originally used for the validation simulations.

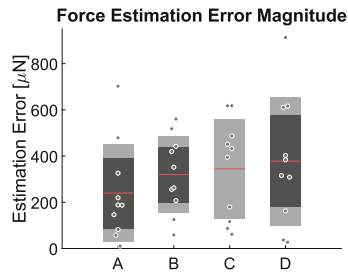


**Fig. 6.** Force estimation error for four muscle actuators on a substrate. Error is the absolute value of the difference of the model's force estimations and force value of the validation point. Mean value (red line), one standard deviation from the mean (dark grey region), 95% t-interval for mean (light grey). (Color figure online)



**Response Surface Performance.** The Response Surface method had an error of  $321 \pm 219 \mu\text{N}$  and a maximum error of  $913 \mu\text{N}$  (Fig. 6). One-way ANOVA showed no statistically significant difference between the force estimation error of different muscles ( $p = 0.555$ ). This model takes days to train on 200 force input sets, but  $79.8 \pm 51.9$  s for each force set estimation, with four muscles per set.

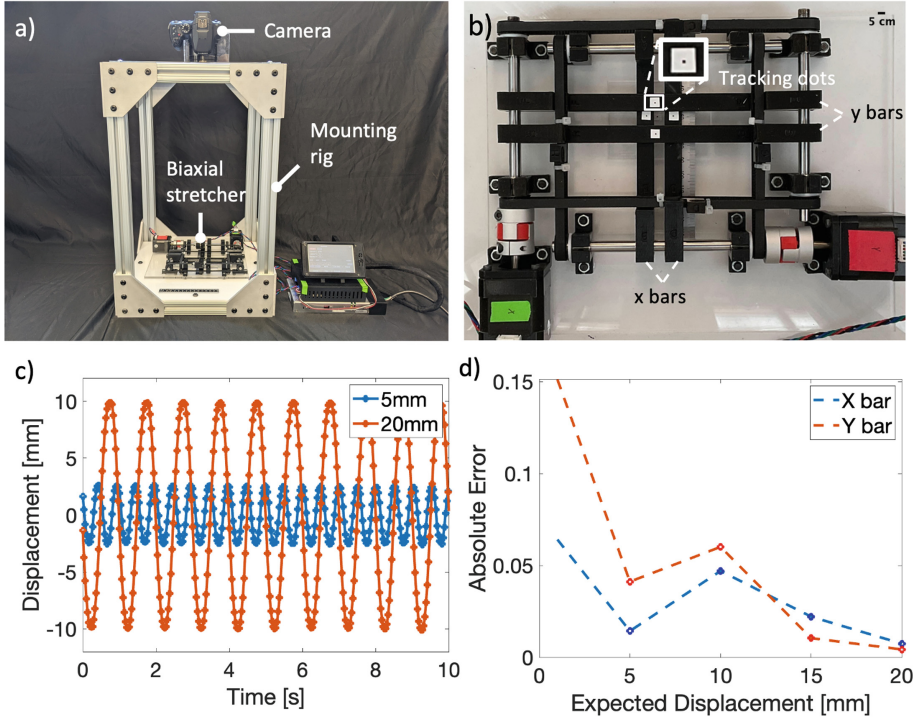
**Direction Optimization Performance.** The Direct Optimization method had an average and maximum error of  $0 \mu\text{N}$ . This occurred because the method could keep updating its estimation of muscle forces until the resulting mesh deformation matched the input mesh deformation exactly. If this model were evaluated on *in vitro* measurements of mesh deformation, we would expect it to have some error arising from the discrepancies between the mechanics captured in the finite element model and the actual mechanics of the embodied distributed muscle actuation mesh construct. This model does not require training but does take  $663.4 \pm 918.5$  s for each force set estimation. Comparing Response Surface and Direct Optimization methods, one-way ANOVA shows a difference in their force estimation error ( $p \ll 0.001$ ) when aggregating the muscles' force estimations within each model.

### 3.3 Characterization and Performance of Biaxial Stretching Platform

Using the experimentally identified adjustment ratio to more closely achieve desired displacements, our biaxial stretching platform achieved an average positioning error of  $3.10 \pm 5.92\%$  and  $5.34 \pm 2.38\%$  for the x- and y-axis, respectively. The uniform adjustment value was used for short displacements (5, 10) and the displacement-specific adjustment was used for longer displacements (15, 20). The average relative positioning error is higher for shorter displacements and tends to decrease as the displacement increases (Fig. 7c). The error value for higher displacements, 15 mm and 20 mm, had low displacement error, of less than 2.5%. The highest displacement error was 0.64 mm for the y-bar at 20 mm displacement. Since future experimental validations involve using displacements values in this higher range, the biaxial stretching platform performance is promising. The precision of the biaxial stretcher was also characterized, as it is important to know how repeatable a given displacement can be achieved. Over a ten second trial, the displacement oscillation maintains a consistent movement profile (Fig. 7d), which is an important requirement for future validation of the computational tools. Table 1 details this repeatability, showcasing low standard deviations for the system across all commanded displacements.

**Table 1.** Mean  $\pm$  standard deviation of measured displacements for four commanded displacements.

Commanded (mm)	Measured (mm, x-bars)	Measured (mm, y-bars)
5 mm	$4.75 \pm 0.17$	$5.03 \pm 0.10$
10 mm	$10.22 \pm 0.34$	$10.53 \pm 0.14$
15 mm	$15.08 \pm 0.33$	$14.87 \pm 0.18$
20 mm	$19.78 \pm 0.12$	$19.84 \pm 0.37$

**Fig. 7.** a) Mounting rig housing biaxial stretcher and camera. b) Four tracked points on each attachment bar of the biaxial stretcher. c) Representative plots of displacement vs time for biaxial stretcher y-bar. d) Plot of the absolute error ratio vs displacement for x- and y-bars.

## 4 Conclusion

The work presented here suggests that our computational tools can achieve contactless strain and force estimation of distributed muscle actuators patterned on a mesh substrate based on mesh deformation. We show that the placement and orientation of muscle actuators on a stretched mesh substrate affect the strain those muscles experience. We also present two methods for extracting force

estimations from distributed muscle actuators patterned on a mesh substrate. The first method, Response Surface Optimization, outputs force estimations quickly after model training, but has high error between its estimations and the computationally generated validation force sets. The second method, Direct Optimization, generates force estimations approximately 8 times slower, but provides more precise estimations. Towards validation of the estimation approaches, an experimental platform was constructed that can apply known deformations to a polymer mesh and will feature known forces applied by springs as analogs for muscle forces. To improve the strain estimation method—as well as both force estimation methods—future work will include materials testing to refine the material model of the mesh substrate to be more representative of collagen. Following validation, these methods will support *in vitro* experiments towards the design and fabrication of a biohybrid meshworm robot.

**Acknowledgements.** This material is based on work supported by a Carnegie Mellon University (CMU) Dean’s Fellowship as well as National Science Foundation Graduate Research Fellowship Program under grant No. DGE1745016 and by the National Science Foundation CAREER award program (grant no. ECCS-2044785). The authors would also like to acknowledge Ian Turner for his work on design and assembly of the camera mounting rig and Brian Bock for helpful comments on the manuscript.

## References

1. Tracker Video Analysis Tool. <https://physlets.org/tracker/>
2. Designxplorer user guide (2019). <https://ansyshelp.ansys.com/>
3. Genetic aggregation (2020). <https://ansyshelp.ansys.com/>
4. MOGA Workflow MOGA Steps to Generate a New Population (2020)
5. Ben Salem, M., Roustant, O., Gamboa, F., Tomaso, L.: Universal prediction distribution for surrogate models. *Soc. Ind. Appl. Math.* **5**, 1086–1109 (2017)
6. Boxerbaum, A.S., Shaw, K.M., Chiel, H.J., Quinn, R.D.: Continuous wave peristaltic motion in a robot. *Int. J. Robot. Res.* **31**(3), 302–318 (2012)
7. Cvetkovic, C., et al.: Three-dimensionally printed biological machines powered by skeletal muscle. *PNAS* **11**(28), 10125–10130 (2014)
8. Donnelly, K., Khodabukus, A., Philp, A., Deldicque, L., Dennis, R.G., Baar, K.: A novel bioreactor for stimulating skeletal muscle *in vitro*. *Tissue Eng. Part C Methods* **16**(4), 711–718 (2010)
9. Hinds, S., Bian, W., Dennis, R.G., Bursac, N.: The role of extracellular matrix composition in structure and function of bioengineered skeletal muscle. *Biomaterials* **32**(14), 3575–3583 (2011)
10. Horchler, A.D., et al.: Peristaltic locomotion of a modular mesh-based worm robot: precision, compliance, and friction. *Soft Robot.* **2**(4), 135–145 (2015)
11. Ingber, D.E.: Cellular mechanotransduction: putting all the pieces together again. *FASEB J.* **20**(8), 811–827 (2006)
12. Islam, A., Chapin, K., Younesi, M., Akkus, O.: Computer aided biomanufacturing of mechanically robust pure collagen meshes with controlled macroporosity. *Biofabrication* **7**(3), 035005 (2015)
13. Kandhari, A., Wang, Y., Chiel, H.J., Daltorio, K.A.: Turning in worm-like robots: the geometry of slip elimination suggests nonperiodic waves. *Soft Robot.* **6**(4), 560–577 (2019)

14. Lee, K.Y., et al.: An autonomously swimming biohybrid fish designed with human cardiac biophysics. *Science* **375**(6581), 639–647 (2022)
15. Mammoto, T., Mammoto, A., Ingber, D.E.: Mechanobiology and developmental control. *Annu. Rev. Cell Dev. Biol.* **29**(1), 27–61 (2013)
16. Morimoto, Y., Onoe, H., Takeuchi, S.: Biohybrid robot powered by an antagonistic pair of skeletal muscle tissues. *Sci. Robot.* **3** (2018)
17. Nawroth, J.C., et al.: A tissue-engineered jellyfish with biomimetic propulsion. *Nat. Biotechnol.* **30**(8), 792–797 (2012)
18. Pagan-Diaz, G.J., et al.: Simulation and fabrication of stronger, larger, and faster walking biohybrid machines. *Adv. Func. Mater.* **28**(23), 1–13 (2018)
19. Park, S.J., et al.: Phototactic guidance of a tissue-engineered soft-robotic ray. *Science* **353**(6295), 158–162 (2016)
20. Powell, C.A., Smiley, B.L., Mills, J., Vandeburgh, H.H.: Mechanical stimulation improves tissue-engineered human skeletal muscle. *Am. J. Physiol. Cell Physiol.* **283**(5), 1557–1565 (2002)
21. Raman, R., et al.: SI: damage, healing, and remodeling in optogenetic skeletal muscle bioactuators. *Adv. Healthc. Mater.* **6**(12) (2017)
22. Rangarajan, S., Madden, L., Bursac, N.: Use of flow, electrical, and mechanical stimulation to promote engineering of striated muscles. *Ann. Biomed. Eng.* **42**(7), 1391–1405 (2014). <https://doi.org/10.1007/s10439-013-0966-4>
23. Ricotti, L., et al.: Biohybrid actuators for robotics: a review of devices actuated by living cells. *Sci. Robot.* **2** (2017)
24. Selman Sakar, M., et al.: Formation and optogenetic control of engineered 3D skeletal muscle bioactuators. *Lab Chip* **23**, 4976–4985 (2012)
25. Seok, S., Onal, C.D., Cho, K.J., Wood, R.J., Rus, D., Kim, S.: Meshworm: a peristaltic soft robot with antagonistic nickel titanium coil actuators. *IEEE/ASME Trans. Mechatron.* **18**(5), 1485–1497 (2013)
26. Shiwardski, D.J., Tashman, J.W., Eaton, A.F., Apodaca, G., Feinberg, A.W.: 3D printed biaxial stretcher compatible with live fluorescence microscopy. *HardwareX* **7**, e00095 (2020)
27. Turner, D.Z.: Digital image correlation engine (DICE) reference manual, Sandia report, SAND2015-10606 O. Technical report, Sandia report (2015). <https://github.com/dicengine/dice>
28. Webster, V.A., et al.: *Aplysia Californica* as a novel source of material for biohybrid robots and organic machines. In: Lepora, N.F.F., Mura, A., Mangan, M., Verschure, P.F.M.J.F.M.J., Desmulliez, M., Prescott, T.J.J. (eds.) *Living Machines 2016*. LNCS (LNAI), vol. 9793, pp. 365–374. Springer, Cham (2016). [https://doi.org/10.1007/978-3-319-42417-0\\_33](https://doi.org/10.1007/978-3-319-42417-0_33)
29. Webster, V.A., Hawley, E.L., Akkus, O., Chiel, H.J., Quinn, R.D.: Effect of actuating cell source on locomotion of organic living machines with electrocompacted collagen skeleton. *Bioinspiration Biomimetics* **11**(3), 036012 (2016)
30. Webster-Wood, V.A., Akkus, O., Gurkan, U.A., Chiel, H.J., Quinn, R.D.: Organismal engineering: toward a robotic taxonomic key for devices using organic materials. *Sci. Robot.* **2**(12), 1–19 (2017)